Characterization of nanostructured GaSb: comparison between large-area optical and local direct microscopic techniques

I. S. Nerbø,[1,*] M. Kildemo,[1] S. Le Roy,[2] I. Simonsen,[1,2] E. Søndergård,[2] L. Holt,[1] and J. C. Walmsley[1]

[1]Department of Physics, Norwegian University of Science and Technology (NTNU), NO-7491 Trondheim, Norway

[2]Surface du Verre et Interfaces, Unité Mixte de Recherche CNRS/Saint-Gobain Laboratoire, UMR 125, 39 Quai Lucien Lefranc, F-93303 Aubervilliers Cedex, France

*Corresponding author: ingar.nerbo@ntnu.no

Received 28 May 2008; accepted 13 August 2008;
posted 21 August 2008 (Doc. ID 96717); published 24 September 2008

Low energy ion-beam sputtering of GaSb results in self-organized nanostructures with the potential of structuring large surface areas. Characterization of such nanostructures by optical methods is studied and compared to direct (local) microscopic methods. The samples consist of densely packed GaSb cones on bulk GaSb, approximately 30, 50, and 300 nm in height, prepared by sputtering at normal incidence. The optical properties are studied by spectroscopic ellipsometry, in the range 0.6–6.5 eV, and with Mueller matrix ellipsometry in the visible range, 1.46–2.88 eV. The optical measurements are compared to direct topography measurements obtained by scanning electron microscopy, high resolution transmission electron microscopy, and atomic force microscopy. Good agreement is achieved between the two classes of methods when the experimental optical response of the short cones ($<$55 nm) is inverted with respect to topological surface information, via a graded anisotropic effective medium model. The main topological parameter measured was the average cone height. Optical methods are shown to represent a valuable characterization tool of nanostructured surfaces, in particular when a large coverage area is desirable. Because of the fast and nondestructive properties of optical techniques, they may readily be adapted to *in situ* configurations.

OCIS codes: 120.2130, 160.4236, 310.6628, 260.2065.

1. Introduction

The recent advent of nanotechnology and nanoscience has made it increasingly important to be able to "see" features of a sample down to a nanometric scale. Today this is typically achieved with the aid of several well-established microscopic techniques like, atomic force microscopy (AFM), scanning electron microscopy (SEM) and transmission electron microscopy (TEM). All these techniques can achieve nanometric resolution, and are therefore attractive when one wants to image the fine details of a sample. Moreover, they can be said to be *local* in the sense that only a rather small surface area can be imaged with good resolution. They are also rather time consuming techniques, and the required equipment is costly and physically large. As a result, they are not generally suited for *in situ* characterization.

Traditionally, optical techniques have been attractive for *in situ* studies due to its measurement speed, relatively low equipment cost, noncontact properties, and ease of integration with other setups. Optical techniques also have the advantage of being able to cover a large surface area with relative ease. This is a great advantage, for instance, in monitoring applications where it is the average properties that are of interest, and not the local features at a given

0003-6935/08/285130-10$15.00/0

location at the surface. For nanometer scale structures, the applicability of optical techniques are limited by the diffraction limit [1], making imaging of such structures by visible light impossible. However, even if direct optical imaging is challenging for nanostructures, it is well-known that they can have strong polarization altering properties on the incident radiation. Hence, indirect optical techniques can, in principle, be devised for the purpose of extracting topographic information about the sample. The aim of this paper is to present such a methodology, and to compare the large area optical result to local information obtained by direct methods.

Spectroscopic ellipsometry (SE) is a celebrated polarimetric technique, much used for measuring the thickness of thin film layers and for determining the index of refraction of materials. It can also be used to characterize nanostructures. For example, generalized ellipsometry has been used to measure the inclination angle of nanorods [2]. The sensitivity of spectroscopic ellipsometry to the thickness of thin layers is remarkable and can be down to single atom layers. This is achieved by knowing the refractive indices of the materials and utilizing optical models. The aim of this study is to exploit SEs sensitivity of thin film thickness to accurately measure the height of conical shaped nanostructures. This is done by developing a suitable optical model. Information on shape and regularity can possibly also be attained. The ellipsometric spot will always average over a relatively large (surface) area, providing information on the mean properties of the structures. It is both noninvasive and fast, making it suitable as a tool for *in situ* characterization.

Nanostructured surfaces and materials open up for a new range of applications. In photonics, for example, optical properties of thin films may be mimicked by nanostructures and supply new and enhanced properties (see e.g., [2], and references therein). An example of such properties can be antireflective coatings with low reflectivity over a large spectral range and a wide range of incident angles [3].

Low energy ion sputtered GaSb is a good example of self-organized formation of densely packed cones and has been proposed as a cost-effective method for production of e.g., quantum dots [4]. The properties of such a surface may, to a large extent, be tailored by controlling sputtering conditions. The latter issue is a typical target application area of ellipsometry. In the case of a future large scale production of such surfaces, SE could possibly be used as an efficient production control tool for testing individual samples.

Here, optical models are initially constructed from observations from high resolution transmission electron microscopy (HR-TEM), field emission gun scanning electron microscopy (FEG-SEM), and AFM. The latter give a direct observation of the nanostructures, with respect to density, cone separation, cone height, number of nearest neighbors, etc. Information on the shape and crystal structure of individual cones, were obtained from HR-TEM studies of carefully prepared slices of nanostructured GaSb.

This paper is organized as follows: In Section 2 we describe the experimental details of both the direct microscopic (SEM, TEM, and AFM), and the optical (SE) studies. A brief theoretical background on ellipsometry is also given. In Section 3 we present the results of these studies. The optical properties of conical nanostructures are discussed in relation to the effective medium approximation. An optical model is presented in Subsection 3.C that enables characterization of such structures from optical measurements by fitting the model parameters to the SE measurements. Information gained from optical characterization are finally compared to the results from the direct microscopic studies.

2. Experimental Details and Theoretical Background

The samples consisted of GaSb sputtered by low energy Ar^+ ions [5]. The sputtering conditions for each sample are reported in Table 1. The substrates were crystalline GaSb (100) wafers of 500 μm thickness. All samples were sputtered at room temperature. The samples characterized in this study (samples A–D) were all sputtered at normal ion incidence. Additional samples were also prepared by sputtering at 45° ion incidence, resulting in nanocones tilted from the surface normal [6]. Characterization of such structures are left for future work. The FEG-SEM images were obtained using a Hitachi S-4300SE, and Zeiss Supra instruments. TEM analysis was performed using a JEOL 2010F. Cross section TEM samples were prepared by both ion-milling and ultramicrotomy to investigate possible preparation induced artefacts in the microstructure. Ion-milling was performed using a Gatan PIPS instrument, operating at 3.5 kV with a thinning angle of 3.5–4°. Ultramicrotomy was performed using a Reichart–Jung Ultracut E instrument. AFM measurements were done by a DI-VEECO AFM with a NanoScope IIIa controller from Digital Instruments, operated in tapping mode. Silicon tips with radius less than 10 nm were used.

The optical far field measurements were performed using a commercial photo-elastic-modulator spectroscopic ellipsometer (PMSE) in the photon energy range 0.6–6.5eV (UVISEL, Horriba Jobin Yvon), at an angle of incidence of 55°. The complete Mueller matrix was also measured using a commercial ferroelectric liquid-crystal retarder-based Mueller matrix

Table 1. Sputtering Conditions and Definition of the Samples

Sample Name	Sputter Time (min)	Mean Temperature (°C)	Applied Voltage (V)	Average Flux (mA/cm^2)
A	10	33	−400	0.098
B	10	41	−400	0.096
C	10	35	−300	0.28
D	10	47	−500	0.37

ellipsometer (MM16) in the range 1.46–2.88 eV (850–430 nm). Such measurements were made for several angles of incidence in the range from 55° to 70° and as a function of the sample rotation angle around its normal to the (mean) surface. The orientation of the sample with respect to the direction of the incoming beam was carefully recorded, and the sample was rotated manually in steps of 45(±2)°, with a total sample rotation in all cases of at least 360°.

The PMSE measurements were performed in the standard UVISEL setup, i.e., a polarizer-sample-PEM-analyzer, where the angle of the fast axis of the PEM with respect to the analyzer is fixed at 45°. Measurements were performed in the standard PMSE configurations ($\Theta_M = 0°$, $\Theta_A = 45°$) [7], determining $I_s = -m_{43}$ and $I_c = m_{33}$, where m_{43} and m_{33} are normalized Mueller matrix elements related to the unormalized Mueller matrix M by $m = M/M_{11}$. For the reflection from an isotropic planar surface, they can be defined according to

$$I_s = -m_{43} = \sin 2\Psi \sin \Delta, \tag{1}$$

$$I_c = m_{33} = \sin 2\Psi \cos \Delta, \tag{2}$$

where Ψ and Δ denote the ellispometric angles related to the ratio of the complex reflection amplitudes $r_{pp}/r_{ss} = \tan \Psi e^{i\Delta}$ [8].

Additional measurements were performed in the configuration ($\Theta_M = 45°, \Theta_A = 45°$), enabling the determination of

$$I_{c_2} = -m_{12} = \cos 2\Psi. \tag{3}$$

The quantities, I_s, I_c, and I_{c_2}, as defined in Eqs. (1)–(3) are known as the ellipsometric intensities. For block-diagonal Mueller matrices, these intensities can be used to define the degree of polarization P [9]:

$$P = \sqrt{I_s^2 + I_c^2 + I_{c_2}^2}. \tag{4}$$

A discussion on when a sample will have a block-diagonal Mueller matrix will be given in the Section 3. From the full Mueller matrix, experimentally available here in the range 1.46–2.88 eV, it is also customary to define the so-called depolarization index (consult, e.g., Ref. [10] for a more detailed discussion of depolarization measures):

$$D_P = \frac{\sum_{ij} M_{ij}^2 - M_{11}^2}{\sqrt{3} M_{11}}, \tag{5}$$

where M_{ij} denotes the nonnormalized Mueller matrix elements [10]. P (and in most cases D_P) determine how much of the outgoing light will be totally polarized for totally-polarized incident light. Reflectance measurements were also performed by the PMSE, in which $M_{11} = (R_{ss} + R_{pp} + R_{sp} + R_{ps})/2$ was determined by using a standard Al mirror reference sample, and assuming stable intensity conditions. The reflectance spectrum was recorded from 1.5–6.5 eV in steps of 0.1 eV.

3. Results and Discussion

A. Experimental Observations—SEM, TEM, and AFM Results

In Fig. 1, FEG-SEM images of samples A and D are presented, for both normal beam incidence (left-hand images), and tilted beam incidence (right-hand images). The cones do not show a high degree of organization but, on average, have 6 neighbors. This result was found from statistical treatment of AFM measurements of the samples, but could as well have been found from SEM images. The result corresponds well with the Euler law [11], which states that the mean number of nearest neighbors for a structure created by a random process is 6. The average cone separation $\langle D \rangle$ has been estimated from the cone density, by assuming the cones are ordered on a perfect hexagonal lattice. The average heights of the cones $\langle h \rangle$ were nominally estimated from AFM, but for sample A it was estimated from HR-TEM. The average cone heights and cone separations are given in Table 2, along with the estimated standard deviation σ_h of $\langle h \rangle$.

Figure 2 depicts a HR-TEM image of selected cones from sample A prepared by ion-milling. The average cone height of A was estimated to be 55 nm, obtained by taking the average of 16 cones measured by HR-TEM. The shape was found to be conical with a somewhat rounded tip. The typical cone angle, defined as the angle between the substrate and the cone side wall, was found to be roughly $\alpha = 73°$. From the HR-TEM images in Fig. 2, it is observed that the

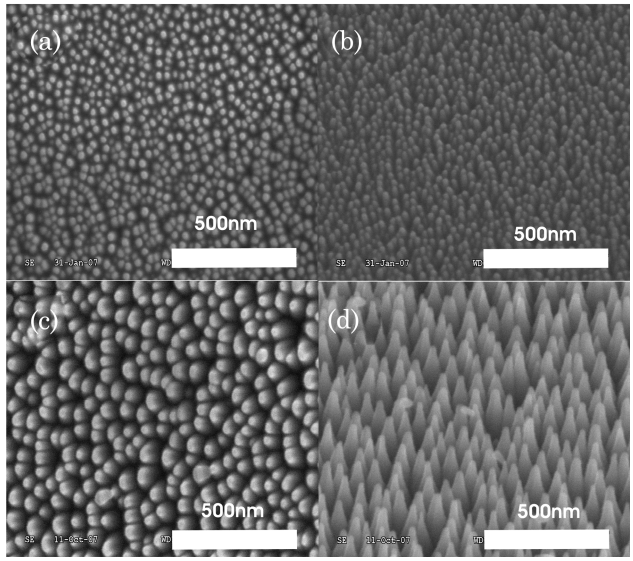

Fig. 1. SEM images of GaSb nanocones.(a) Sample A at normal beam incidence, (b) tilted sample A. Sample D is also depicted at (c) normal beam incidence and (d) tilted beam incidence.

Table 2. Results of AFM, TEM, and SEM Studies of GaSb Nanocone Samples

Sample Name	$\langle h \rangle$ (nm)	σ_h (nm)	Density (μm^2)	$\langle D \rangle^*$ (nm)	α (degree)
A	55 [b]	5.4 [b]	549 [c]	46 [c]	73 [b]
B	46.5 [c]	5.2 [c]	948 [c]	35 [c]	
C	47.6 [c]	8.85 [c]	766 [c]	39 [c]	
D	299 [d]	40 [d]	74.25[c]	125 [c]	77.2 [d]

[a] $\langle h \rangle$ is the average cone height, with standard deviation σ_h. Density is the number of cones per μm, D is the average distance between neighboring cone centers, while α is the average cone angle. The tabulated results have been found from the following:
[b] TEM studies.
[c] AFM measurements.

interior of the cones consisted of primarily crystalline material, with the same crystal orientation as the substrate. Furthermore, the cone surface appeared to be surrounded by a thin (less than 5 nm) layer of undetermined amorphous material. From the rapid oxidation of clean GaSb to an approximately 5–7nm GaSb-oxide layer, it is argued that this surrounding layer is partially oxidized.

Another slice of nanostructured GaSb (sample A) , was prepared by ultramicrotomy. This sample did not provide such a thin sector as the ion-milled samples. However, it was sufficient to confirm the structure observed in the ion-milled samples. The crystalline nature of the interior of the cones and the amorphous surrounding layer is in line with the observations by Facsko *et al.* [4].

In summary, from the TEM studies mainly three phases appear to be involved in the layer (thin film) defined by the cones. These phases are crystalline GaSb (c-GaSb), amorphous GaSb (a-GaSb), and presumed GaSb-oxide, in addition to the voids between the cones. The remaining samples were studied by AFM and by FEG-SEM, and detailed results are compiled in Table 2. It is suspected that the AFM tip is too blunt to reach the bottom between close-packed cones. Therefore, when estimating average cone height $\langle h \rangle$, the height of each cone top has been defined relative to the lowest point in an area within the maximal distance between the cones. This minimum is typically found in a place where the cones stand further apart, and the tip can reach the bottom. This may overestimate average height $\langle h \rangle$ somewhat.

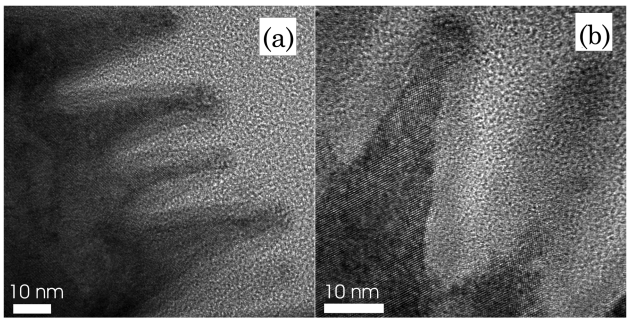

Fig. 2. High resolution TEM images of GaSb nanocones (sample A). Figure (a) shows several cones while figure (b) shows one individual cone in greater detail. The lighter part of the image is the amorphous adhesive used in the sample preparation. The crystalline cones appear darker and in (b) the atomic column spacing at the 110 GaSb zone-axis orientation is clearly visible. The approximately 5 nm layer of amorphous GaSb oxide is visible as a shadow around the cones that has slightly darker contrast than the adhesive.

B. Experimental Observations—Spectroscopic Ellipsometry

Figure 3 shows the SE measurements of $I_s = -m_{43}$, $I_c = m_{33}$ of a clean GaSb surface with approximately 7 nm of oxide. In addition it shows, as an overview, the ellipsometric measurements of samples A, B, C (short cones), and D (longer cones). All cones were formed by sputtering at normal incidence. The nanostructuration of the surface strongly modifies the polarization-dependent optical response. Another interesting feature is the reflectance of such nanostructured surfaces, which have additional practical applications. It is particularly clear from Fig. 4 that the reflectance is much reduced, compared to the clean surface, at higher photon energies. Furthermore, the antireflection properties tend to appear for lower energies as the cones get higher. This could be explained as a motheye effect from the graded index of refraction [12].

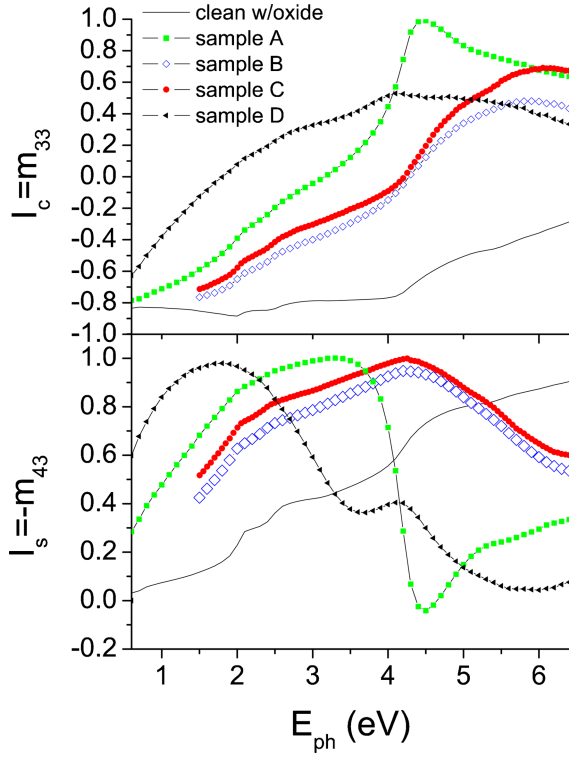

Fig. 3. (Color online) Ellipsometric intensities $I_s = -m_{43}$, $I_c = m_{33}$, of plane GaSb with 7 nm oxide, short nanostructured cones, samples A, B, and C (approximately 50 nm high cones), and sample D (approximately 300 nm cones).

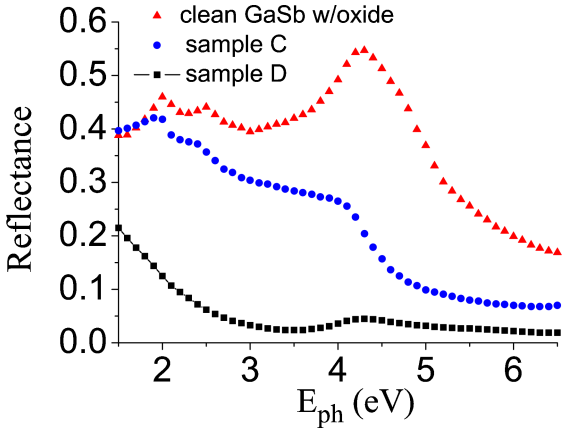

Fig. 4. (Color online) Reflectance (M_{11}) of nanostructured GaSb cones, for sample C (approximately 36 nm high cones) and D (approximately 300 nm high cones). As a reference, the reflectance of a clean GaSb surface with oxide is also included.

From FEG-SEM and HR-TEM images, it is observed that the samples consist of conical nanostructures of various sizes. For sufficiently small cones, the surface can be treated as a thin film layer of effective medium. This layer will be uniaxially anisotropic since the cones will show a different response to an electric field normal to the mean surface than to a field parallel to it. Anisotropic uniaxial materials with the optic axis in the plane of incidence will appear like an isotropic material under ellipsometric investigations ($r_{sp} = r_{ps} = 0$) [13], in the sense that reflections from such materials will be described by a diagonal Jones matrix, and by a block-diagonal Mueller–Jones matrix. This means that all the polarization altering properties of the structured surface can be described by the ellipsometric angles Ψ and Δ, derived from the ellipsometric intensities I_s and I_c.

Cones being directed normal to the surface have a symmetry axis that is normal to the mean surface, and the approximated effective media must therefore have an optic axis in the same direction, i.e., it will appear like an isotropic material and can be fully characterized by regular (standard) ellipsometry. The samples will then have full azimuth rotation symmetry (around the sample normal). If the cones are tilted from the sample normal, this will generally no longer be the case (except for the two special azimuth orientations where the tilted cones lie in the plane of incidence). The structures will then correspond to an anisotropic material with a tilted optic axis. To describe the polarizing properties of reflections from such a surface, one also needs to account for the coupling of the s and p polarization through the reflections coefficients r_{sp} and r_{ps}, in addition to r_{pp} and r_{ss}. A long range ordering, or anisotropic shapes of the individual cones, would also break the rotation symmetry and give polarization coupling. To fully characterize such a sample, one needs to perform generalized ellipsometry (see e.g., [14,15]) or Mueller matrix ellipsometry. Mueller matrix ellipsometry has a great advantage over generalized ellipsometry, since it also can deal with depolarizing samples, which is not the case for the latter. Depolarization may arise from irregularities in the structure (shape, size, and ordering) and from multiple scattering. If the cones are small enough to be treated by effective medium theory, the structures will have the same effect as layers that are homogeneous in a plane parallel to the surface, and there will be no multiple scattering. When the dimensions of the cones exceed the validity of the effective medium theory, the inhomogeneities will give rise to multiple scattering and depolarization. In this case there will be coupling between the polarization modes even though the structures are rotationally symmetric and point normal to the surface, since the structures no longer can be approximated as an effective homogeneous layer. From this observation, one may conclude whether a given sample can be modeled accurately by effective medium theory from measurements of depolarization alone.

To examine if the samples give polarization coupling, their Mueller matrices measured by MME have been analyzed. If there is no coupling, the Mueller matrix should be block diagonal. We define a measure of the degree of nonblock diagonality as

$$A = \left(\frac{m_{13}^2 + m_{14}^2 + m_{23}^2 + m_{24}^2 + m_{31}^2 + m_{32}^2 + m_{41}^2 + m_{42}^2}{m_{11}^2 + m_{12}^2 + m_{21}^2 + m_{22}^2 + m_{33}^2 + m_{34}^2 + m_{43}^2 + m_{44}^2} \right)^{1/2}, \tag{6}$$

which is 0 for block-diagonal Mueller matrices (such as reflections from isotropic surfaces), and has the value 1 for maximum nonblock-diagonal matrices (such as circular polarizers and ±45 linear polarizers). Figure 5 shows this quantity as a function of azimuth sample rotation around the mean surface normal for various samples. Additionally, as a reference, a sample with nanostructures sputtered at 45°

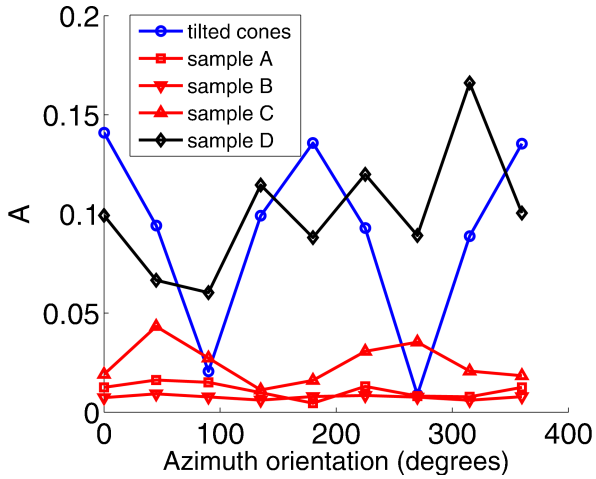

Fig. 5. (Color online) Degree of nonblock diagonality (A, as defined in Eq. (6) for various samples, as a function of azimuth sample rotation, for $E_{ph} = 2.75$ eV. The sample denoted tilted cones consisted of cones tilted 45° from the surface normal (approximately 30 nm high), while the other samples have cones pointing normal to the surface.

of incidence, with an effective layer thickness of approximately 30 nm is also shown [6,16]. This sample consists of cones tilted by approximately 45° from the mean surface normal and has as expected a Mueller matrix that is only block diagonal for azimuthal orientations where the cones lie in the plane of incidence.

Moreover, it is observed from Fig. 5, that the short cone samples have negligible polarization coupling, while the longer cones have substantial deviations from a block-diagonal Mueller matrix. This coupling could, as earlier discussed, be related to a slight tilting of the cones, a long range preferential ordering of the cones, or an anisotropic shape of the individual cones. It is speculated that a long range preferential ordering could be induced by e.g., substrate polishing features. However, for sample D, no azimuthal orientation has been observed to give a block-diagonal Mueller matrix, as should be the case for a thin film with the optic axis in the plane of incidence. This implies that these samples cannot be modeled as an anisotropic thin film layer, and that their optical properties are strongly affected by multiple scattering. Such samples cannot be fully characterized by SE, and full Mueller matrix ellipsometry is instead necessary. Samples A, B, and C only show a slight deviation from block-diagonal Mueller matrices, and these off-diagonal elements will be neglected in the following analysis and modeling. The detailed analysis and modeling of tilted cones will be treated in a separate publication [16].

From the polarization coupling at various azimuth orientations of sample D it was concluded that the polarization altering properties of this sample had contributions from multiple scattering, and that it would not be well approximated as an effective medium. From this conclusion, one would expect the sample to be depolarizing, which is confirmed by the depolarization index (D_P, defined in Eq. (5) evaluated from the MME measurements (Fig. 6). As expected, depolarization increases for increasing photon energy since the effective medium approximation gets less accurate for decreasing wavelengths. In addition, an approximation to depolarization at higher energies has been found by calculating degree of polarization P from the PMSE measurements through Eq. (4). The degree of polarization obtained in this way is a measure of how much certain polarization states are depolarized and will generally differ from the depolarization index, which (in many cases) is the average depolarization of all possible incident polarization states (see Ref. [10]). For samples with block-diagonal Mueller matrices (A, B, C), the degree of polarization can safely be used as a measure of depolarization. It is observed that the short cones have principally low depolarization throughout the measured spectral range (Fig. 6). All the samples studied in the present work show an increasing depolarization towards the UV range. Sample A has a small dip in the degree of polarization at the photon energy where $I_s = 0$ and $I_c = 1$. This effect can be explained

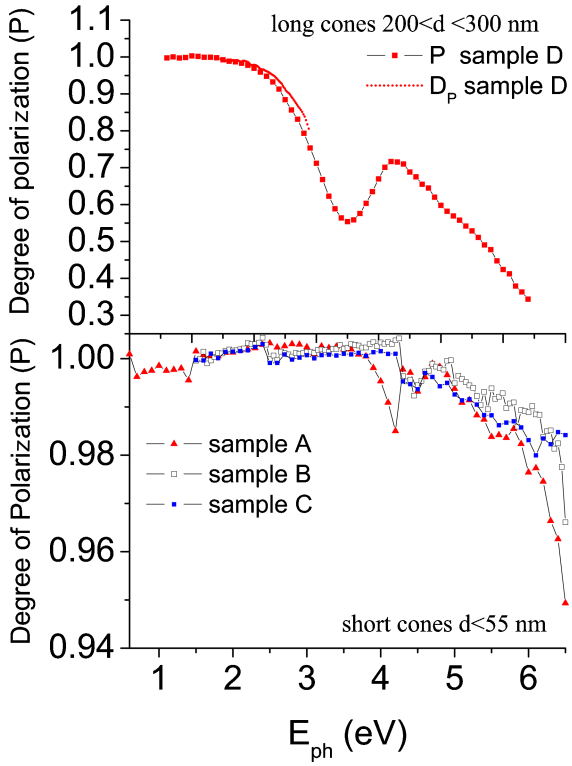

Fig. 6. (Color online) Degree of polarization P, as calculated from the PMSE measurements by Eq. (4), for the nanostructured GaSb samples. The bottom figure shows P for the short cone samples: A, B, and C, while the top figure shows P for the long cones of sample D. The depolarization index D_P, calculated from the Mueller matrix in the visible range, is also shown for the long cones in the top figure.

by a small variation in cone height (thin film thickness) [9] or cone shape. It could also be caused by quasi-monochromatic light from the monochromator. It is especially noted that the dielectric function is descending steeply at this photon energy [17], meaning that a very small wavelength distribution could give depolarization. It is noted that samples B and C show little depolarization in the main part of the spectrum. This does not imply that these samples have less variation in cone height or shape than sample A, since there is no photon energy for which $I_s = 0$ and $I_c = 1$ (see Fig. 3). All the short cones still show a small but observable increasing depolarization for decreasing wavelength. Furthermore, it is observed that degree of polarization P decreases more rapidly as a function of wavelength as the cone height increases.

C. Optical Modeling

Because of the anisotropic shape of the nanostructures, they cannot be modeled by a standard isotropic effective medium theory. The cones with no or little depolarization (short cones) have been modeled as a graded anisotropic thin film layer of effective media on a GaSb substrate. Reflection coefficients have been calculated by an implementation of the Schubert algorithm [18] for reflections from arbitrarily

anisotropic layered systems, based on Berreman 4 × 4 differential matrices [19]. As a first approximation, the cones have been modeled as a stack of cylinders with decreasing diameter. Each cylinder in the stack defines a layer with a homogeneous effective dielectric function. With a sufficient number of layers, this will be a good approximation of a graded thin film layer. Based on HR-TEM observations, we have assumed the cylinders to consist of a core of crystalline GaSb, covered by a coating consisting of a mixture of amorphous GaSb and GaSb oxide. Simpler models consisting only of crystalline GaSb and void have been tested, and were found to not sufficiently explain the measurements. Anisotropy is introduced by using the generalized Bruggeman effective medium theory [20], giving the formula

$$f_{c\text{–GaSb}}\frac{\epsilon_{c\text{–GaSb}}-\epsilon_{ii}}{\epsilon_{ii}+L_i(\epsilon_{c\text{–GaSb}}-\epsilon_{ii})}+f_{\text{coat}}\frac{\epsilon_{\text{coat}}-\epsilon_{ii}}{\epsilon_{ii}+L_i(\epsilon_{\text{coat}}-\epsilon_{ii})}+f_{\text{void}}\frac{\epsilon_{\text{void}}-\epsilon_{ii}}{\epsilon_{ii}+L_i(\epsilon_{\text{void}}-\epsilon_{ii})}=0, \tag{7}$$

where f and ϵ denote the filling factors and complex dielectric functions, respectively, with the subscript c – GaSb referring to the crystalline core, coat to the coating over layer, and void to the surrounding void. L_i denotes the depolarization factor in direction i (along a principal axis of the structure) and ϵ_{ii} is the effective dielectric function in direction i. Our principal axes will be two orthogonal axes parallel to the mean surface, x and y, and a z axis normal to the mean surface. The dielectric function of the coating, ϵ_{coat}, has been determined by letting it be a mixture of amorphous GaSb (a-GaSb) and GaSb oxide (oxide), and using the standard Bruggeman equation for spherical inclusions ($L_i = 1/3$):

$$f_{a\text{–GaSb}}\frac{\epsilon_{a\text{–GaSb}}-\epsilon_{\text{coat}}}{\epsilon_{\text{coat}}+2\epsilon_{a\text{–GaSb}}}+f_{\text{oxide}}\frac{\epsilon_{\text{oxide}}-\epsilon_{\text{coat}}}{\epsilon_{\text{coat}}+2\epsilon_{\text{oxide}}}=0. \tag{8}$$

These cylinders can thus be approximated as an effective thin film layer, which is valid when the distances between neighboring cylinders are much smaller than the wavelength of the light. The layer will be anisotropic, with depolarization factor $L_x = L_y = 0.5$ in the plane parallel to the surface, and $L_z = 0$ in the direction normal to the surface. The reflection coefficients from such an anisotropic layered system have been calculated and used to find the ellipsometric intensities I_s and I_c [8]:

$$I_s = \frac{2\,\mathrm{Im}(r_{pp}r_{ss}^* + r_{ps}r_{sp}^*)}{|r_{ss}|^2+|r_{pp}|^2+|r_{sp}|^2+|r_{ps}|^2}, \tag{9}$$

$$I_c = \frac{2\,\mathrm{Re}(r_{pp}r_{ss}^* + r_{ps}r_{sp}^*)}{|r_{ss}|^2+|r_{pp}|^2+|r_{sp}|^2+|r_{ps}|^2}. \tag{10}$$

The parameters of the models have been fitted to I_s and I_c by minimizing χ^2, defined as

$$\chi^2 = \frac{1}{2N-M+1}\sum_{i=1}^{N}\left[\frac{(I_{si}^{\text{mod}}-I_{si}^{\text{exp}})^2}{\sigma_{si}^2}+\frac{(I_{ci}^{\text{mod}}-I_{ci}^{\text{exp}})^2}{\sigma_{ci}^2}\right], \tag{11}$$

where N and M are the number of measurement points and the number of free parameters in the model, respectively. σ_{si} and σ_{ci} are the standard deviations of the respective measurements. Additional measurements such as any Mueller matrix element, or the reflectance, may be added to the formulae in a similar fashion.

The simplest model giving satisfactory results has been one with 5 parameters (see Fig. 7): total height h; relative (effective) diameters D_1 and D_2 of the bottom and top cylinder cores; thickness of the coating s; and amount of oxide in the coating f_{oxide}. Diameters D_1 and D_2 and thickness s are dimensionless quantities, defined as fractions of the mean nearest neighbor distance of the cones. This distance cannot be found from the optical measurements when the effective medium approximation is valid, since the effective medium only depends on volume filling factors and shape through depolarization factors L_i. This means that the model is independent of the scale in the horizontal plane for all structures sufficiently smaller than the wavelength of light. A stack of $\mathcal{N} = 100$ cylinders of equal height were used to approximate a continuous gradient, with the diameters $d(n)$ of layer n decreasing linearly from D_1 to D_2:

$$d(n) = D_1 - \frac{D_1 - D_2}{\mathcal{N}-1}n, \tag{12}$$

for $n = 0, 1, \ldots, 99$. Assuming a hexagonal ordering of the cylinders, the filling factor of crystalline GaSb and coating become

$$f_{c\text{–GaSb}}(n) = \frac{\pi}{\sqrt{12}}\mathrm{d}^2(n), \tag{13}$$

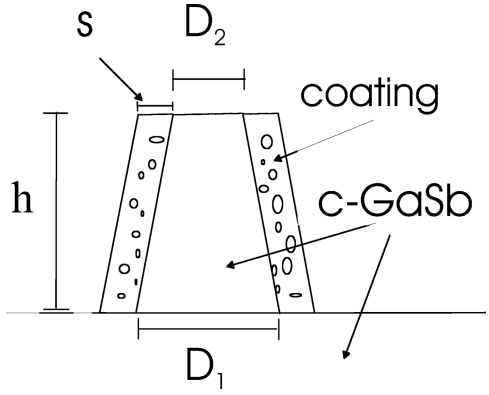

Fig. 7. Parameters used in the graded effective medium model. h is the total height, s is the thickness of the coating of amorphous material and oxide, D_1 and D_2 are the lower and upper diameters of the crystalline core.

$$f_{\text{coat}}(n) = \frac{2\pi}{\sqrt{3}}[\mathrm{d}(n)s + s^2]. \quad (14)$$

Notice that for an effective medium theory it is only the filling factors that play a role, and not the specified ordering of the cones. As long as the filling factors remain the same, effective medium theory cannot distinguish between different geometric arrangements. The distance between the centers of neighboring cones has been set to unit length. The thickness of coating is constant for all layers.

Minimization was performed using the sequential quadratic programming (SQP) algorithm of the Matlab Optimisation Toolbox 3.1.1. The dielectric functions of crystalline GaSb, amorphous GaSb, and GaSb oxide were obtained from the literature [17,21,22]. The standard deviations (noise) σ_{si} and σ_{ci} of the ellipsometric measurements I_s and I_c were estimated to be 0.01.

The modeled ellipsometric intensities are presented together with the measurements in Figs. 8 and 9, with the model parameters given in Table 3. The model gave a good fit to the optical measurements of sample A (Fig. 8), with a cone height of 54 nm and a clear grading in the inner cylinder diameters from $D_1 = 0.55$ to $D_2 = 0.36$. This is in good agreement with the previously presented SEM and TEM images (see Fig. 2). Two simpler models consisting only of crystalline GaSb and void are also shown in Fig. 8: one where the cones are modeled as cylinders, and one where they are modeled as a stack of cylinders with decreasing radius. Niether of them gave a satisfactory result.

Sample C could be well fit by a model with $D_1 \approx D_2$, meaning that it could have been modeled equally well by only one layer of coated cylinders. The cone height was found to be 36 nm. It may be that the optical measurements are not sensitive to a possible gradient in such a short structure, or that the structures have a shape resembling a cylinder.

The ellipsometric measurements of sample B greatly resemble those of sample C but the optical model could not give an equally good fit. When D_1 and D_2 are allowed to vary freely, the model converges to a seemingly unphysical case (based on the TEM, and SEM images) with $D_2 > D_1$. To avoid this problem, they have been constrained so that $D_1 > D_2$. The result is then a cylinder-like model (no grading), with a height of 32 nm. It may appear to be necessary to develop more advanced models to perfectly fit the measurements of this sample. Natural extensions could be to let the coating thickness s vary with height, letting the diameter $d(n)$ of layer n follow a nonlinear function from D_1 to D_2, or by letting the filling factors be able to deviate from values consistent with a hexagonal ordering. We do not, however, treat such advanced models here, but keep the parameters in the models to a minimum for easier interpretation and to avoid unphysical solutions. It is also plausible that the dielectric functions of the different phases mixed in the effective medium theory are somehow different, e.g., that the properties of the oxide are different.

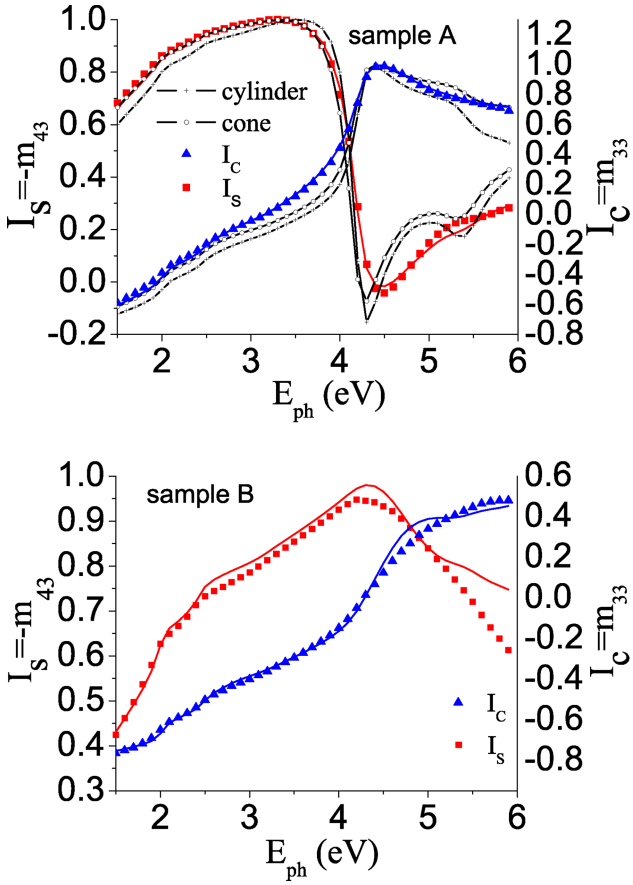

Fig. 8. (Color online) Simulated and experimental ellipsometric intensities $I_s = -m_{43}$ and $I_c = m_{33}$, for sample A (top) and sample B (bottom). The filled squares and filled triangles are the measured I_s and I_c, respectively. The solid lines are the simulated values calculated from the fitted model, with parameters defined in Fig. 7 (sample A: $\chi^2 = 2.6$, sample B: $\chi^2 = 12.4$). For sample A, simpler models with only crystalline material in the effective medium layer have also been included for comparison. The lines marked by crosses (+) are for a model made by treating the cones as cylinders ($\chi^2 = 118$), the lines marked by circles (○) are for a graded model as described in Fig. 7, but with no coating of oxide and amorphous material ($\chi^2 = 61.7$).

Table 3. Resulting Parameters from Fitting the Optical Models to the Ellipsometric Data

Sample Name	h (nm)	D_1	D_2	s	f_{oxide}	χ^2	f_{tot}
A	54	0.55	0.36	0.10	0.56	2.6	0.39
B	32	0.31	0.31	0.21	0.64	12.4	0.46
C	36	0.36	0.35	0.14	0.34	1.1	0.37
D [b]	165	0.95	0.21	0	0.0	7.4	0.34

[a] h is the total height of the model layers, D_1 and D_2 are the bottom and top diameter of the crystalline core, respectively, s is the coating thickness, and f_{oxide} is the amount of oxide in the coating. χ^2 is the square deviation of the modeled ellispometric intensities from the measured, as defined in Eq. (11). D_1, D_2, and s are defined relative to the center to center distance for two nearest neighbors.

[b] Sample D was only curve fitted below 2.5 eV (i.e., for $P > 0.9$).

According to the results from the optical characterization, sample B should consist of slightly shorter cones than sample C. This seems overall consistent with the AFM observations. It has been observed for samples A, C, and D that the nearest neighbor distance increases for increasing cone height (Table 2). From the cone density one should therefore expect sample B to have shorter cones than sample C. The average cone height $\langle h \rangle$ estimated from AFM did not show as clear a difference between the samples, but such small height differences could possibly be masked in the uncertainty in the estimation of $\langle h \rangle$.

The height of the cones of samples B and C obtained from the optical model are lower than the average heights found by AFM. It should be stressed that the heights of sample A (which coincided well with the height from the optical model) were found in a different way (by HR-TEM). As previously mentioned, the average cone height estimated from AFM measurements may be exaggerated. The model appears to be very sensitive to changes in the thickness of the effective medium layer, a perturbation in thickness of only a few nm results in a large increase of χ^2. However, different models may result in different layer thicknesses. For instance, it may seem more reasonable to let the cones be covered by a coating of thickness s also on the top. This has been tested and resulted in equally good χ^2 values as the models reported in Table 3 but with total heights 4–5 nm higher. The problem with such a model is that the thickness of the coating top layer has to be determined absolutely, not just as a ratio, s, of the nearest neighbor distance. This distance cannot be obtained from SE measurements but must be found from e.g., AFM or SEM studies. We are interested in a model that can help us characterize the nanostructures from SE measurements alone, and therefore reject this model with a coating also on the top.

The total volume filling factors for the optical models are tabulated in the last column of Table 3. For ideal cones, ordered in a hexagonal lattice, the maximal filling factor is 0.30. The model filling factors lie in the range 0.34–0.46, in good correspondence to the rounded conical structures observed from TEM, SEM, and AFM measurements (rounded cones will give a larger filling factor than cones with a sharp top). Exact estimation of filling factors from microscopy images proved to be difficult. The varying shape and size of the individual cones must be taken into account, together with the mean nearest neighbor distance. The AFM measurements should in principle be ideal for this, but because of a too blunt tip and holes in the surface, they drastically overestimate the filling factors. By estimating the shape and size of an individual cone from a TEM image, and using the mean nearest neighbor distance from AFM measurements, a rough estimation of the filling factor of sample A was found to be 0.36 ± 0.04, in reasonable agreement with the value from the optical model (0.39).

The construction of an effective medium optical model, predicts structural parameters that correspond reasonably well to the physical height of the samples, and the density/shape of the cones. Equally important, the models can by used to predict optical properties not measured. The model of sample A, calibrated by SE measurements at 55° angle of incidence, were used to successfully predict results of SE measurements at 70° angle of incidence. The models may also predict the reflectance (R_{ss}, R_{pp}, or R) of the samples (see Fig. 9). We propose that the models can be used as a tool to calculate the polarization dependent optical properties of such samples at any angle of incidence.

The large depolarizing properties of sample D indicate that it may not be modeled appropriately by effective medium theory over the full spectral range considered. The experimental observations represent an interesting case, in the sense that there are no commonly available models to appropriately fit these data. A tentative effective medium modeling between 0.6 and 2.5 eV was tested to extract

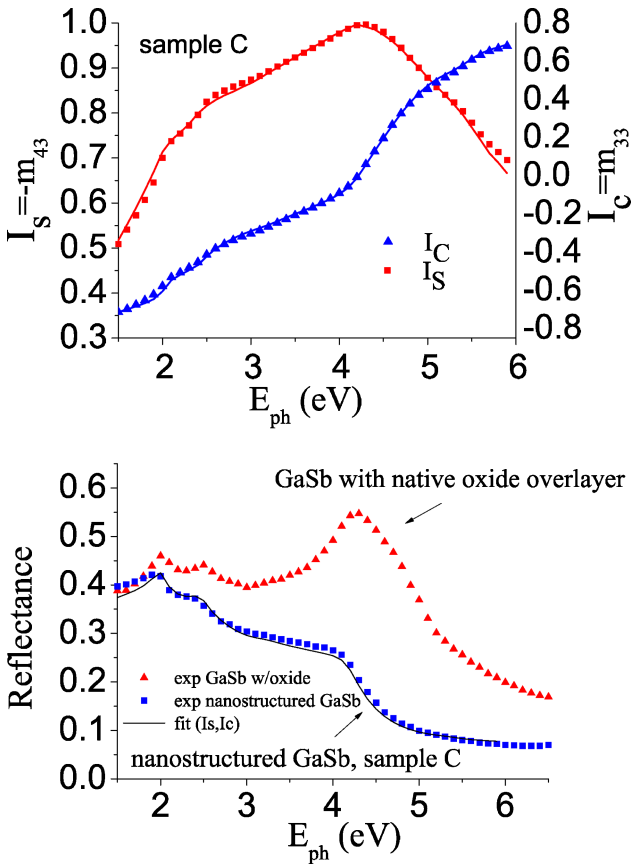

Fig. 9. (Color online) Simulated and experimental ellipsometric intensities $I_s = -m_{43}$ and $I_c = m_{33}$, for sample C (top). The filled squares and filled triangles are the measured I_s and I_c, respectively. The solid lines are the simulated values calculated from the fitted model, with parameters defined in Fig. 7 (sample C: $\chi^2 = 1.1$). The bottom figure depicts the measured reflectance $R = (|r_{ss}|^2 + |r_{pp}|^2)/2$ [filled squares for sample C, filled triangles for GaSb with native oxide layer)], and simulated reflectance, calculated from the fitted model.

approximately the cone height of sample D. It was found to be 165 nm, about half of the height found by SEM but still considerably higher than heights found for the short cones and with a clear gradient. The dielectric function data for GaSb oxide and c-GaSb in the photon energy range 0.6–1.5 eV were not available in the literature and were, therefore, extrapolated from PMSE measurements at 70° angle of incidence. The parameters of the resulting model are tabulated for completeness. Improved optical models suitable for modeling of the optical response of these samples are currently being undertaken and planned for future work.

4. Summary and Conclusions

Spectroscopic ellipsometry and Mueller matrix ellipsometry have been shown to be useful techniques for the characterization of nanostructured surfaces, such as nanocones of GaSb on GaSb. Overall, the observations from SE appear to be consistent with the results from SEM, TEM, and AFM studies. An optical model has been found to fit well to the measurements obtained for short cones (of height 55 nm and lower). This was achieved by treating the structures as a graded anisotropic thin film of effective medium. These models have been applied to obtain an approximation to the average cone height of the samples and also, to some extent, to gain information on the cone shape. They may also be used to estimate reflectance and polarization altering properties for reflections at any angle of incidence. The nanostructuration of the surface was shown to considerably reduce the reflectance. The antireflecting properties increased with cone height. Samples with long nanocones (200–300 nm) were found to be strongly depolarizing and could not be modeled as an effective medium. The full Mueller matrix must be measured to fully characterize the polarization altering properties of such samples. We have demonstrated that SE can be a fast and nondestructive way of characterizing nanocones of GaSb with the possibilities of *in situ* control under production.

The authors are grateful to M. Stchakovsky at Horiba Jobin Yvon for access to scientific instruments, and Susanne W. Hagen at NTNU for doing complementary measurements.

References

1. M. Born and E. Wolf, *Principles of Optics. Electromagnetic Theory of Propagation, Interference and Diffraction of Light*, 6th corrected ed. (Pergamon, 1980).
2. G. Beydaghyan, C. Buzea, Y. Cui, C. Elliott, and K. Robbie, "*Ex situ* ellipsometric investigation of nanocolumns inclination angle of obliquely evaporated silicon thin films," Appl. Phys. Lett. **87**, 153103 (2005).
3. Z. P. Yang, L. Ci, J. A. Bur, S. Y. Lin, and P. M. Ajayan, "Experimental observation of an extremely dark material made by a low-density nanotube array," Nano Lett. **8**, 446–451 (2008).
4. S. Facsko, T. Dekorsy, C. Koerdt, C. Trappe, H. Kurz, A. Vogt, and H. L. Hartnagel, "Formation of ordered nanoscale semiconductor dots by ion sputtering," Science **285**, 1551–1553 (1999).
5. N. Brun, A. Lelarge, S. Le Roy, E. Søndergård, and E. Barthel are preparing a manuscript to be called "Composition of nanostructured GaSb."
6. M. Kildemo, I. S. Nerbø, E. Søndergård, L. Holt, I. Simonsen, and M. Stachakovsky, "Optical response of nanostructured gasb," Phys. Stat. Sol C **5**, 1382–1385 (2008).
7. B. Drévillon, "Phase modulated ellipsometry from the ultraviolet to the infrared: *in situ* applications to the growth of semiconductors," Prog. Cryst. Growth Charact. **27**, 1–87 (1993).
8. P. Hauge, "Conventions and formulas for using the Mueller–Stokes calculus in ellipsometry," Surf. Sci. **96**, 81–107 (1980).
9. G. E. Jellison, Jr. and J. W. McCamy, "Sample depolarization effects from thin films of ZnS on GaAs as measured by spectroscopic ellipsometry," Appl. Phys. Lett. **61**, 512–514 (1992).
10. R. A. Chipman, "Depolarization index and the average degree of polarization," Appl. Opt. **44**, 2490–2495 (2005).
11. D. Weaire and N. Rivier, "Soap, cells and statistics—random patterns in two dimensions," Contemp. Phys. **25**, 59–99 (1984).
12. C. G. Bernhard, "Structural and functional adaptation in a visual system," Endeavour **26**, 79–84 (1967).
13. R. M. A. Azzam and N. M. Bashara, *Ellipsometry and Polarized Light* (North-Holland, 1987).
14. G. E. Jellison and F. A. Modine, "Two-modulator generalized ellipsometry: theory," Appl. Opt. **36**, 8190–8198 (1997).
15. A. Laskarakis, S. Logothetidis, E. Pavlopoulou, and M. Gioti, "Mueller matrix spectroscopic ellipsometry: formulation and application," Thin Solid Films **455–456**, 43–49 (2004).
16. I. S. Nerbø, M. Kildemo, S. W. Hagen, S. Leroy, and E. Søndergård, "Optical properties and characterization of tilted gasb nanocones," (to be published).
17. D. E. Aspnes and A. A. Studna, "Dielectric functions and optical parameters of Si, Ge, GaP, GaAs, GaSb, InP, InAs, and InSb from 1.5 to 6.0 ev," Phys. Rev. B **27**, 985–1009 (1983).
18. M. Schubert, "Polarization-dependent optical parameters of arbitrarily anisotropic homogeneous layered systems," Phys. Rev. B **53**, 4265–4274 (1996).
19. D. W. Berreman, "Optics in stratified and anisotropic media: 4 × 4 matrix formulation," J. Opt. Soc. Am. **62**, 502–510 (1972).
20. J. E. Spanier and I. P. Herman, "Use of hybrid phenomenological and statistical effective-medium theories of dielectric functions to model the infrared reflectance of porous sic films," Phys. Rev. B **61**, 10437–10450 (2000).
21. J. Stuke and G. Zimmerer, "Optical properties of amorphous iii-v compounds. i. Experiment," Phys. Stat. Sol. B **49**, 513–523 (1972).
22. S. Zollner, "Model dielectric functions for native oxides on compound semiconductors," Appl. Phys. Lett. **63**, 2523–2524 (1993).